Nanoscale

Accepted Manuscript

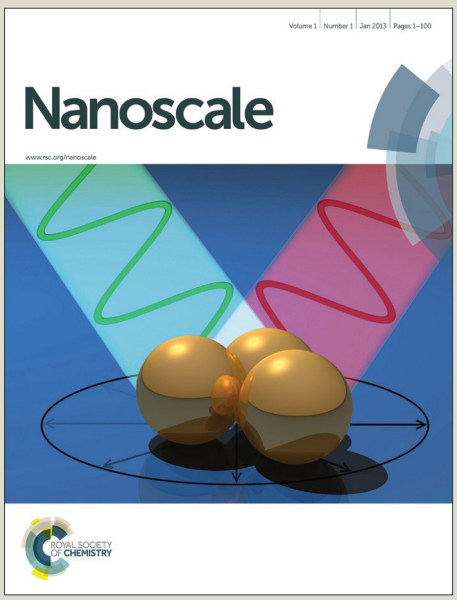

ROYAL SOCIETY OF CHEMISTRY

www.rsc.org/nanoscale

Journal Name

RSCPublishing

COMMUNICATION

Charge-Sensitive Fluorescent Nanosensors Created from Nanodiamond†

Cite this: DOI: 10.1039/x0xx00000x

V. Petrakova,[a, b]* I. Rehor,[c] J. Stursa,[d] M. Ledvina,[a,c] M. Nesladek,[a,e,f] and P.Cigler[c]*

Received 00th January 2012,
Accepted 00th January 2012

DOI: 10.1039/x0xx00000x

www.rsc.org/

We show that fluorescent nanodiamonds (FNDs) are among the few types of nanosensors that enable direct optical reading of noncovalent molecular events. The unique sensing mechanism is based on switching between the negatively charged and neutral states of NV centers which is induced by interaction of FND surface with charged molecules.

A nitrogen-vacancy (NV) center is a point lattice defect in a diamond consisting of a substitutional nitrogen atom and a vacancy at an adjacent lattice point. This color center is a near-infrared emitter providing a broad emission peak with a maximum at ~700 nm.[1] Unlike other fluorophores, NV centers provide exceptionally stable fluorescence and do not photobleach or blink even after extreme continuous excitation used for example in super-resolution fluorescence microscopy.[2] NV centers thus represent a promising alternative to small-molecule labels, fluorescent proteins, and quantum dots. Fluorescent nanodiamonds (FNDs) bearing NV centers have been used in biology primarily as non-toxic fluorescent labels in cell[3–10] and animal[11,12] bioimaging. Moreover, electron transitions between NV quantum states can be manipulated using microwave radiation at ~2.87 GHz which results in changes in its emission intensity that can be further modulated by external magnetic field.[1,13] This behavior can be measured using optically detected magnetic resonance (ODMR), which has been used for construction of FND-based sensors for detection of electric[14] or magnetic[13] field, for NV tracking with precision of several nanometers[15] as well as for chemosensing[16] even in living cells.[17]

Here, we provide evidence that FNDs containing NV centers are among the few types of nanosensors that enable direct optical reading of noncovalent binding events based on modulation of fluorescence. Moreover, their specificity to detect changes in charge goes significantly beyond the functionality offered by conventional fluorescent nanoprobes. In contrast to techniques that require special setups (such as ODMR), fluorescence reading can be performed routinely with a confocal microscope or spectrofluorimeter.

Although many highly sensitive and selective nanoparticle-based detection systems for biomolecular detection have been developed, they often include cytotoxic reagents and work only "in tube".[18] In contrast, only a limited number of signaling modes is available for intracellular and *in vivo* applications. These include mainly resonance energy transfer (Förster, bioluminescence, and chemiluminescence resonance energy transfer), charge transfer in semiconductor nanoparticles, modulation of localized surface plasmon resonance and surface-enhanced Raman scattering.[19] Recently, it was reported that the emission state of NV centers in FNDs can be controlled by changing the ND surface chemistry at an atomic level.[20–24] NV centers in NDs exist in two electronic states: negatively charged (NV^-) and neutral (NV^0). The NV^- state emits in the red region with zero phonon line (ZPL) at 637 nm, which is followed by broad phonon replica side band luminescence with the highest intensity around 700 nm. The NV^0 state emits orange luminescence with ZPL around 575 nm, also followed by similar broad side bands.[1] The reversible switching between the NV^- and NV^0 states is enabled by shifting the position of the NV^0 and NV^- ground state levels with respect of the Fermi level at the ND surface. Thus, when the NV^- ground state level is shifted below the Fermi level, an electron is lost from the NV center and *vice versa*. Depending on the surface termination, complementary changes in the occupancy of the NV^- and NV^0 energy states occur, which consequently affect the shape of fluorescence spectra.[20–22,25]

We hypothesized that manipulations of the ND surface that affect the NV^- and NV^0 states are not limited to changes in atomic surface composition, but also include interactions in aqueous solution. We therefore designed a set of fundamental experiments to test whether surface-charge-induced modulation of fluorescence can be observed for noncovalent surface chemical processes. Next, we explored an approach for direct two-color fluorescent monitoring of molecular binding events in proximity to the ND surface, which is an essential feature for construction of future ND-based fluorescent biosensors. For the experiments we used previously described FNDs[26] of mean diameter ~49 nm and containing on average 1.7 NVs per particle (see Supporting Information and Figure S1 for experimental details and particle characterization).

We took advantage of the high level of polymer adsorption on NDs[27] and created a well-controlled model system for binding of macromolecules to ND surfaces. By simply incubating NDs with various polymers, we achieved the desired surface changes without the need to construct sophisticated recognition architectures. Based on the previous findings that the NV^- state is more populated in oxidized, negatively charged NDs,[20–22,25] we focused on ND surface charge reversal upon binding cationic polymers, which should lead to depletion of NV^- occupancy and subsequent decrease in its emission intensity.

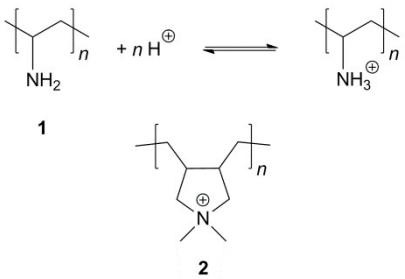

Scheme 1 Structure of poly(allylamine) (**1**), poly(diallyldimethylammonium) cation (**2**), and representation of the reversible protonation of **1**.

To control the surface charge density after adsorption, we chose two types of flexible linear polymers: poly(allylamine) (**1**) and poly(diallyldimethylammonium chloride) (**2**; Scheme 1). While amino groups in **1** can participate in acid-basic equilibria (average $pK_a = 9.7$[28]) and reversibly switch between positively charged and neutral states, the charge of the quaternary ammonium salts is always positive and inert to pH changes.

First, we focused on confirming the electrostatic adsorption of polymers **1** and **2** onto the FND surface. We measured the pH dependence of the particles' zeta potentials, which correspond to the electrical potentials near the nanoparticle surface at the "slipping plane" – the border between bulk water and the tightly adsorbed hydration sphere (Figure 1).

The zeta potential of oxidized FNDs was negative over the entire pH range tested (Figure 2). The highly acidic FND surface[29] resisted full protonation even at strongly acidic pH (pH ≈ 2). Upon addition of cationic polymers, the zeta potential reversed from –40 mV to +40 mV, confirming successful binding of polymers on the FND surface. However, at higher pH, the zeta potential of the FND-**1** complex began to drop due to gradual deprotonation of the surface-bound polymer. The FND-**1** complex thus dynamically responds to changes in pH and allows us to manipulate charge density on the FND surface. The zeta potential of the FND-**2** complex remained positive and roughly constant over the entire pH range.

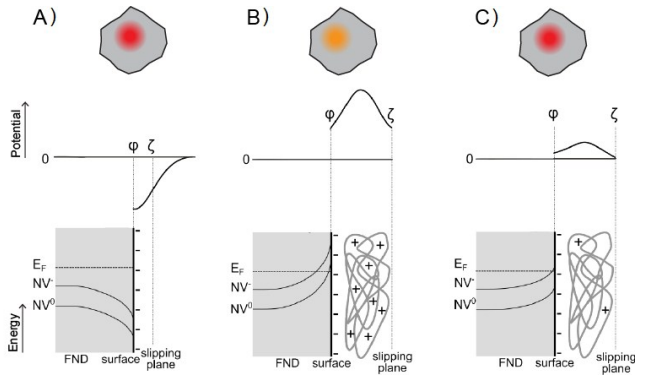

Fig. 1 Schematic representation of zeta potentials and the electronic band structure near the FND surface. The colour codes of the FND particles (purple/orange) correspond to true FND emission colours. A) Bare oxidized FND and its interactions with B) a cationic polymer, and C) a deprotonated cationic polymer. E_F, Fermi level; energy bands are also shown for the NV^- and NV^0 states; ζ, zeta potential; φ, surface potential. The electronic structures in the lower panels are based on previous calculations.[20]

For FND, FND-**1**, and FND-**2**, we measured the dependence of fluorescence spectra on pH (Figure 3A; for complete data, see Figure S2 in Supporting Information). The spectra show typical shapes with expected ZPLs of the NV^0 (575 nm) and NV^- (638 nm) states accompanied by their characteristic red-shifted phonon replicas (see Figure S3 for full range spectrum of FND).

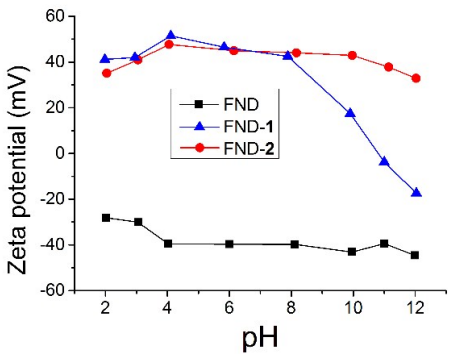

Fig. 2 Dependence of zeta potential of FND and FND-**1** and FND-**2** complexes on pH.

First, we focused on comparing the spectral shapes for FND and FND-**1** and FND-**2** complexes at pH ≈ 6 (Figure 3A). Both polymers are positively charged at this pH, and their binding on

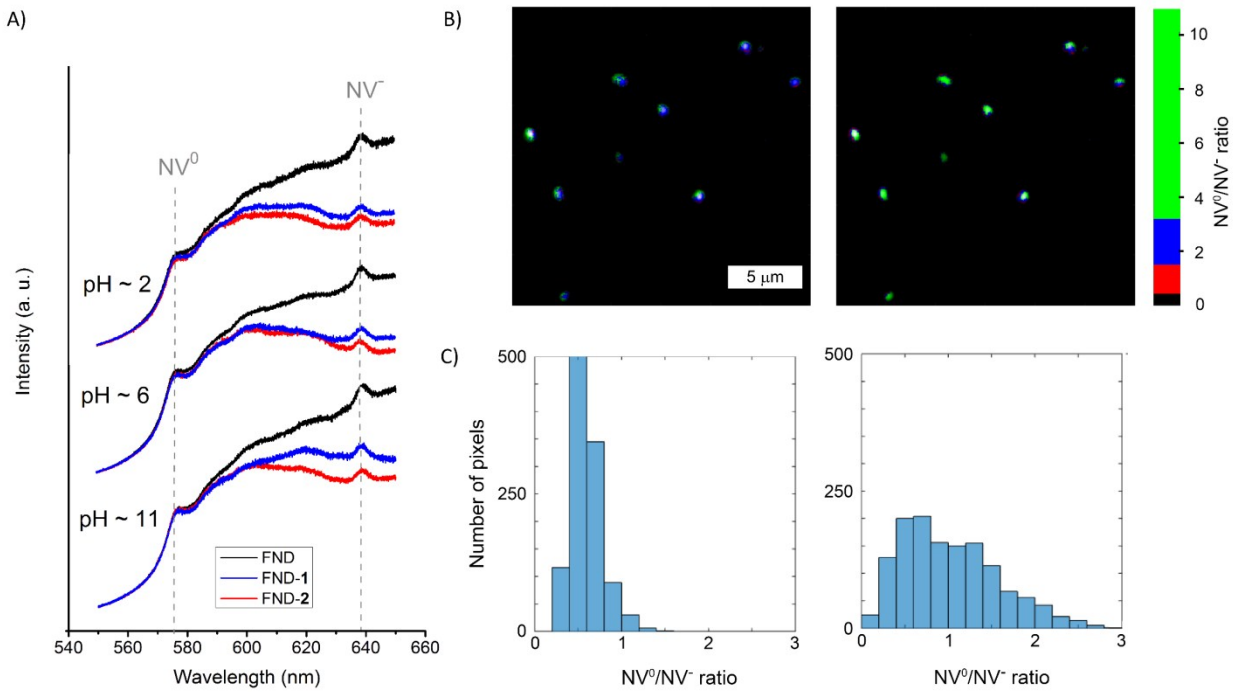

Fig. 3 A) Section of fluorescence spectra involving ZPL of the NV^0 and NV^- states for FND and FND-**1** and FND-**2** complexes measured at pH ≈ 2, 6, and 11. The spectra for each pH are normalized to the NV^0 ZPL. The triads of FND, FND-**1** and FND-**2** spectra are shifted for clarity. B) Fluorescence image showing NV^0/NV^- ZPL fluorescence intensity ratio of FND particles deposited on glass slide covered in droplet of water (left) and of FND-**2** complex (right) formed 10 minutes after addition of **2**. C) Histogram representing the number of pixels per values of NV^0/NV^- ZPL fluorescence intensity ratio for FND (left) and FND-**2** (right). A clear shift to higher NV^0/NV^- ratio after addition of **2** is demonstrated. The total number of pixels was the same in both cases.

the FND surface clearly contributes to depletion of the NV^- band and reduction of its phonon replicas. The situation is analogous for pH ≈ 2, at which the polymers are similarly charged. After alkalization to pH ≈ 11, we observed a difference in the behavior of FND-**1** and FND-**2** complexes. While FND-**2** remains positively charged, FND-**1** loses its charge upon deprotonation (see also Figure 2), the charge density at the FND-**1** interface drops, and the depletion of NV^- emission is therefore weaker for FND-**1**.

For convenient and quantitative representation of these changes, we plotted the $NV^0/(NV^0+NV^-)$ ZPL emission ratios *versus* pH for FND, FND-**1**, and FND-**2** (Figure S2D in Supporting Information). Modulation of fluorescence induced by binding of positively charged polymers on FND surfaces results consistently in a dramatic increase in the $NV^0/(NV^0+NV^-)$ ratio along the entire pH range. The expected decrease of this parameter for FND-**1** in the strongly alkaline region (pH ≈ 11) due to deprotonation was, however, not significant, and the polymers **1** and **2** cannot be distinguished on this base. We also performed analogous control experiments with negatively charged and neutral polymers, revealing that these have indeed an insignificant effect on FND fluorescence (Figure S4 in Supporting Information).

To demonstrate the potential of the sensing mechanism for molecular imaging, we performed a set of experiments on cover slide with deposited FND particles. To avoid the influence of refractive index on the fluorescence intensity, we covered the surface with a water droplet and measured always in aqueous environment. We recorded time-resolved fluorescence from 20x20 μm frame using two spectral regions corresponding to ZPLs of the NV^0 and NV^-. Then we added a small amount of **2**-solution to the water droplet and repeated the measurement with the same particles. We processed the data using intensity and fluorescence lifetime thresholds. For imaging we chose calculated NV^0/NV^- ZPL emission ratios (see Supporting information for details). A clear color shift caused by formation of FND-**2** complex can be seen (compare Figure 3B, left and right). The shift towards higher NV^0/NV^- ZPL emission ratios upon formation of FND-**2** complex is apparent also from histograms in Figure 3C. As a control experiment we recorded similar images for FNDs interacting with a negatively charged polymer (Figure 5S in Supporting information). Both the images and histograms remained in this case without a significant change.

Interestingly, the histograms reflect also heterogeneity in the particle brightness (related mainly to different contents of NV centers per particle) and sensitivity of the individual particles to the observed molecular interactions. Nevertheless, the spectral properties of the system combined with a proper data processing demonstrated to be robust enough for imaging and selective distinguishing the distinctive molecular events (such

as formation of FND complexes with cationic or anionic polymers).

The theoretical model we recently described[20] can explain the observed results (the simplified schematics in Figure 1 can serves as a guideline). The NV^0 and NV^- ground states with energy levels of 1.2 eV and 2.0 eV, respectively, are both below the Fermi level (E_F) inside a FND crystal. However, near the surface, these levels are bent due to the presence of a surface potential. The negatively charged surface of an oxidized diamond with negative zeta potential (Figure 1A) is responsible for downward band bending. Upon adsorption of a positively charged polymer, the surface potential and zeta potential are reversed (Figure 1B), and the NV^0 and NV^- levels are bent upward. Thus, the NV^- state switches to NV^0, resulting in corresponding change in fluorescence. Deprotonation of the FND-**1** complex at basic pH reduces its positive charge density, the upward bending effect is lowered, the NV^- center becomes occupied again, and its emission is partially restored (Figure 1C).

Our sensing mechanism based on surface-charge-induced modulation of fluorescence has several important features. First, it is fundamentally different from methods based on resonance energy transfer, which is a common strategy for fluorescent biosensor construction.[19] Although NV centers allow FRET,[30–32] its efficacy is inversely proportional to the sixth power of the distance between chromophores, and therefore only very small FNDs can be used. Because the proportion of NV^- centers (which roughly corresponds to the brightness) drastically decreases with the FND size,[22] this issue is a major limitation for FND-based FRET sensors. In contrast, the sensitivity of an NV center to surface-charge-induced alterations decreases according to the square of its distance from the surface and can be effective for distances between the NV center and surface up to ~20 nm.[20] Based on this fact, one can expect that even bigger FNDs can be sensitive over the entire volume. This may represent a significant advantage over any type of FRET-based FND sensor (which requires bright sub-10-nm particles) and deserves further examination.

Second, a diamond sensor based on surface-charge-induced modulation of fluorescence will have an intrinsic ratiometric reading mode (i.e., one that includes both reference and measurement signals) because the information is contained in the shape of the emission spectrum and not only in the intensity. Merging the reference and responsive signal into one emitter is possible due to the unique non-photobleachable character of NV centers.

Third, the optical behavior of FNDs is qualitatively different from the majority of other fluorescent nanoparticles: their emission spectra do not show quantum confinement effects known for semiconductor nanomaterials such as quantum dots.[4] Possible size polydispersity of FND particles[33] therefore does not contribute to broadening of fluorescent lines and other spectral features caused by polydispersity at semiconductor fluorescent nanoparticles.[34]

Conclusions

In summary, we describe a new detection mechanism based on modulation of fluorescence induced by changes in the FND surface charge that occur upon noncovalent interaction with charged molecules. In a well-controlled model system, we optically detected gradual changes in charge density on the FND surface caused by deprotonation of a polymer containing amino groups. This sensing mechanism is inherently insensitive to particle size polydispersity and operates as an intrinsic ratiometric system containing a natural non-photobleachable reference. This finding opens new possibilities for construction of biocompatible and extremely photostable two-color fluorescent (bio)nanosensors with potential high-impact applications in nanobiological and medical imaging and chemical sensing. We envision applications in time-unlimited detection of molecular events on FND surfaces, selective recognition of molecules, and quantification of chemical and biochemical entities. We are currently working in these directions such as development of intracellular nanosensors for detection and quantification of prototypal charged biopolymers – nucleic acids.

Notes and references

[a] Faculty of Biomedical Engineering, Czech Technical University in Prague, Sitna sq. 3105, 272 01 Kladno, Czech Republic.
E-mail: vladka.petrakova@gmail.com
[b] Institute of Physics AS CR, v.v.i., Na Slovance 1999/2, 182 21 Prague 8, Czech Republic, Prague 8, Czech Republic.
[c] Institute of Organic Chemistry and Biochemistry AS CR, v.v.i. Flemingovo nam. 2, 166 10 Prague 6, Czech Republic.
E-mail: cigler@uochb.cas.cz
Homepage: www.petrcigler.cz
[d] Nuclear Physics Institute AS CR, v.v.i., 250 68, Rez near Prague, Czech Republic.
[e] IMOMEC division, IMEC, Institute for Materials Research, University Hasselt, Wetenschapspark 1, B-3590, Diepenbeek, Belgium.
[f] Institute for Materials Research, University Hasselt, Martelaarlaan 42, B-3500 Hasselt, Belgium.

† This work was supported by the MZ-VES project Nr. 15-33094A, the 7th Framework EU (project DINAMO), ESF European social fund in the Czech Republic - Investments in Education Development - Grant No.CZ.1.07/2.3.00/20.0306, and FWO project (Flanders Diamond spin-magnetometers and nano- particle FRET sensors). Irradiations of NDs were carried out at the CANAM infrastructure of the NPI AS CR Rez supported through MŠMT project No. LM2011019. We thank Mr. J. Havlik, Mr. M. Gulka and Ms. H. Raabova for their very valuable help and Dr. H. Hoffman for critical proofreading of the manuscript.
Electronic Supplementary Information (ESI) available: experimental details and additional fluorescence spectra. See DOI: 10.1039/c000000x/

1 A. Gruber, A. Dräbenstedt, C. Tietz, L. Fleury, J. Wrachtrup and C. von Borczyskowski, *Science*, 1997, **276**, 2012–2014.
2 S. Arroyo-Camejo, M.-P. Adam, M. Besbes, J.-P. Hugonin, V. Jacques, J.-J. Greffet, J.-F. Roch, S. W. Hell and F. Treussart, *ACS Nano*, 2013, **7**, 10912–10919.

3 Y.-R. Chang, H.-Y. Lee, K. Chen, C.-C. Chang, D.-S. Tsai, C.-C. Fu, T.-S. Lim, Y.-K. Tzeng, C.-Y. Fang, C.-C. Han, H.-C. Chang and W. Fann, *Nat. Nanotechnol.*, 2008, **3**, 284–288.
4 C. C. Fu, H. Y. Lee, K. Chen, T. S. Lim, H. Y. Wu, P. K. Lin, P. K. Wei, P. H. Tsao, H. C. Chang and W. Fann, *Proc. Natl. Acad. Sci.*, 2007, **104**, 727–732.
5 A. Alhaddad, M.-P. Adam, J. Botsoa, G. Dantelle, S. Perruchas, T. Gacoin, C. Mansuy, S. Lavielle, C. Malvy, F. Treussart and J.-R. Bertrand, *Small*, 2011, **7**, 3087–3095.
6 J. Slegerova, M. Hajek, I. Rehor, F. Sedlak, J. Stursa, M. Hruby and P. Cigler, *Nanoscale*, 2015, **7**, 415–420.
7 B.-M. Chang, H.-H. Lin, L.-J. Su, W.-D. Lin, R.-J. Lin, Y.-K. Tzeng, R. T. Lee, Y. C. Lee, A. L. Yu and H.-C. Chang, *Adv. Funct. Mater.*, 2013, **23**, 5737–5745.
8 O. Faklaris, V. Joshi, T. Irinopoulou, P. Tauc, M. Sennour, H. Girard, C. Gesset, J. C. Arnault, A. Thorel and J. P. Boudou, *ACS Nano*, 2009, **3**, 3955–3962.
9 Z. Chu, S. Zhang, B. Zhang, C. Zhang, C.-Y. Fang, I. Rehor, P. Cigler, H.-C. Chang, G. Lin, R. Liu and Q. Li, *Sci. Rep.*, 2014, **4**, 4495.
10 I. Rehor, J. Slegerova, J. Kucka, V. Proks, V. Petrakova, M.-P. Adam, F. Treussart, S. Turner, S. Bals, P. Sacha, M. Ledvina, A. M. Wen, N. F. Steinmetz and P. Cigler, *Small*, 2014, **10**, 1106–1115.
11 R. Igarashi, Y. Yoshinari, H. Yokota, T. Sugi, F. Sugihara, K. Ikeda, H. Sumiya, S. Tsuji, I. Mori, H. Tochio, Y. Harada and M. Shirakawa, *Nano Lett.*, 2012, **12**, 5726–5732.
12 V. Vaijayanthimala, P.-Y. Cheng, S.-H. Yeh, K.-K. Liu, C.-H. Hsiao, J.-I. Chao and H.-C. Chang, *Biomaterials*, 2012, **33**, 7794–7802.
13 J. R. Maze, P. L. Stanwix, J. S. Hodges, S. Hong, J. M. Taylor, P. Cappellaro, L. Jiang, M. V. G. Dutt, E. Togan, A. S. Zibrov, A. Yacoby, R. L. Walsworth and M. D. Lukin, *Nature*, 2008, **455**, 644–647.
14 F. Dolde, H. Fedder, M. W. Doherty, T. Nöbauer, F. Rempp, G. Balasubramanian, T. Wolf, F. Reinhard, L. C. L. Hollenberg, F. Jelezko and J. Wrachtrup, *Nat. Phys.*, 2011, **7**, 459–463.
15 G. Balasubramanian, I. Y. Chan, R. Kolesov, M. Al-Hmoud, J. Tisler, C. Shin, C. Kim, A. Wojcik, P. R. Hemmer, A. Krueger, T. Hanke, A. Leitenstorfer, R. Bratschitsch, F. Jelezko and J. Wrachtrup, *Nature*, 2008, **455**, 648–651.
16 A. Ermakova, G. Pramanik, J.-M. Cai, G. Algara-Siller, U. Kaiser, T. Weil, Y.-K. Tzeng, H. C. Chang, L. P. McGuinness, M. B. Plenio, B. Naydenov and F. Jelezko, *Nano Lett.*, 2013, **13**, 3305–3309.
17 L. P. McGuinness, Y. Yan, A. Stacey, D. A. Simpson, L. T. Hall, D. Maclaurin, S. Prawer, P. Mulvaney, J. Wrachtrup, F. Caruso, R. E. Scholten and L. C. L. Hollenberg, *Nat. Nanotechnol.*, 2011, **6**, 358–363.
18 M. M.-C. Cheng, G. Cuda, Y. L. Bunimovich, M. Gaspari, J. R. Heath, H. D. Hill, C. A. Mirkin, A. J. Nijdam, R. Terracciano, T. Thundat and M. Ferrari, *Curr. Opin. Chem. Biol.*, 2006, **10**, 11–19.
19 P. D. Howes, R. Chandrawati and M. M. Stevens, *Science*, 2014, **346**, 1247390.
20 V. Petrakova, A. Taylor, I. Kratochvilova, F. Fendrych, J. Vacik, J. Kucka, J. Stursa, P. Cigler, M. Ledvina, A. Fiserova, P. Kneppo and M. Nesladek, *Adv. Funct. Mater.*, 2012, **22**, 812–819.
21 V. Petráková, M. Nesládek, A. Taylor, F. Fendrych, P. Cígler, M. Ledvina, J. Vacík, J. Štursa and J. Kučka, *Phys. Status Solidi A*, 2011, **208**, 2051–2056.
22 L. Rondin, G. Dantelle, A. Slablab, F. Grosshans, F. Treussart, P. Bergonzo, S. Perruchas, T. Gacoin, M. Chaigneau, H.-C. Chang, V. Jacques and J.-F. Roch, *Phys. Rev. B*, 2010, **82**, 115449–1–5.
23 C. Bradac, T. Gaebel, C. I. Pakes, J. M. Say, A. V. Zvyagin and J. R. Rabeau, *Small*, 2013, **9**, 132–139.
24 M. Kaviani, P. Deák, B. Aradi, T. Frauenheim, J.-P. Chou and A. Gali, *Nano Lett.*, 2014, **14**, 4772–4777.
25 M. V. Hauf, B. Grotz, B. Naydenov, M. Dankerl, S. Pezzagna, J. Meijer, F. Jelezko, J. Wrachtrup, M. Stutzmann, F. Reinhard and J. A. Garrido, *Phys. Rev. B*, 2011, **83**, 081304.
26 J. Havlik, V. Petrakova, I. Rehor, V. Petrak, M. Gulka, J. Stursa, J. Kucka, J. Ralis, T. Rendler, S.-Y. Lee, R. Reuter, J. Wrachtrup, M. Ledvina, M. Nesladek and P. Cigler, *Nanoscale*, 2013, **5**, 3208–3211.
27 X.-Q. Zhang, M. Chen, R. Lam, X. Xu, E. Osawa and D. Ho, *ACS Nano*, 2009, **3**, 2609–2616.
28 S. Kobayashi, M. Tokunoh, T. Saegusa and F. Mashio, *Macromolecules*, 1985, **18**, 2357–2361.
29 J. T. Paci, H. B. Man, B. Saha, D. Ho and G. C. Schatz, *J. Phys. Chem. C*, 2013, **117**, 17256–17267.
30 J. Tisler, R. Reuter, A. Lämmle, F. Jelezko, G. Balasubramanian, P. R. Hemmer, F. Reinhard and J. Wrachtrup, *ACS Nano*, 2011, **5**, 7893–7898.
31 N. Mohan, Y.-K. Tzeng, L. Yang, Y.-Y. Chen, Y. Y. Hui, C.-Y. Fang and H.-C. Chang, *Adv. Mater.*, 2010, **22**, 843–847.
J. M. Say, C. Bradac, T. Gaebel, J. R. Rabeau and L. J. Brown, *Aust. J. Chem.*, 2012, **65**, 496–503.
I. Rehor and P. Cigler, *Diam. Relat. Mater.*, 2014, **46**, 21–24.
J. R. Caram, H. Zheng, P. D. Dahlberg, B. S. Rolczynski, G. B. Griffin, D. S. Dolzhnikov, D. V. Talapin and G. S. Engel, *J. Chem. Phys.*, 2014, **140**, 084701.